Advanced Composite Materials

ISSN: 0924-3046 (Print) 1568-5519 (Online) Journal homepage: http://www.tandfonline.com/loi/tacm20

Cure strain in thick CFRP laminate: optical-fiber-based distributed measurement and numerical simulation

Y. Ito, T. Obo, S. Minakuchi & N. Takeda

To cite this article: Y. Ito, T. Obo, S. Minakuchi & N. Takeda (2015) Cure strain in thick CFRP laminate: optical-fiber-based distributed measurement and numerical simulation, Advanced Composite Materials, 24:4, 325-342, DOI: 10.1080/09243046.2014.906914

To link to this article: http://dx.doi.org/10.1080/09243046.2014.906914

Advanced Composite Materials, 2015
Vol. 24, No. 4, 325–342, http://dx.doi.org/10.1080/09243046.2014.906914

Cure strain in thick CFRP laminate: optical-fiber-based distributed measurement and numerical simulation

Y. Ito[a]*, T. Obo[a], S. Minakuchi[b] and N. Takeda[b]

[a]*Department of Aeronautics and Astronautics, Graduate School of Engineering, The University of Tokyo, 7-3-1 Hongo, Bunkyo-ku, Tokyo 113-8656, Japan;* [b]*Department of Advanced Energy, Graduate School of Frontier Sciences, The University of Tokyo, 5-1-5 Kashiwanoha, Kashiwa, Chiba 277-8561, Japan*

(*Received 6 August 2013; accepted 18 March 2014*)

This study seeks to clarify the mechanism of strain development in curing a thick composite structure with a temperature distribution in the thickness direction. Strain developed during curing can be separated into two parts according to the causes. One is chemical cure shrinkage of the matrix; the other is thermal shrinkage (or expansion) of the cured composite. Therefore, this study consists of a cure-shrinkage part and a thermal-shrinkage part. In both parts, the curing was monitored with an embedded distributed optical-fiber sensor (pulse-pre-pump Brillouin optical-time-domain analysis, PPP-BOTDA) and analyzed. In the cure-shrinkage strain part, the strain distribution caused by different temperature histories was observed. We confirmed that the lower viscosity part was influenced by the cure shrinkage of the other part and that these phenomena can be analyzed by the visco-elastic cure model. In the thermal-strain part, the amount of total shrinkage strain and the apparent coefficient of temperature expansion distribution were observed in the thickness direction. Warpage of the specimen was also observed. These results were confirmed to be caused by the distribution of temperature and of the fiber volume fraction, V_f.

Keywords: composite; cure monitoring; optical fiber; thick laminate; visco-elastic model

1. Introduction

Carbon-fiber-reinforced plastic (CFRP) structures, which have high specific strength and stiffness, have been used extensively in many industrial fields. An important primary application is in aircraft, where they are applied even to primary structures like the wings and fuselage and are used under harsh environments. The quality of these composite structure parts is a key issue for reliable products. The quality is very dependent on their curing process.[1–3] In particular, in highly loaded structural parts, laminates of considerable thickness are utilized, and the cure temperature is not uniform in the through-thickness direction. The temperature distribution in these thick laminates during curing can cause an unexpected residual strain distribution in cured products. Accordingly, it is necessary to measure and understand curing thick composite structures.

For this purpose, several cure-monitoring techniques and analysis models have been established. Differential scanning calorimetry,[4] dielectrometry,[5] and point-type optical-fiber sensors (including extrinsic Fabry–Perot type sensors,[6,7] Raman

*Corresponding author. Email: yusaku@smart.k.u-tokyo.ac.jp

spectroscopy,[8] and fiber Bragg grating sensors [9–11]) are well-known cure-monitoring techniques. Embedded optical-fiber sensors in particular are considered very useful for measuring the temperature and strain inside a curing structure. They are lightweight and small and rarely affect the mechanical properties of the materials in which they are embedded. However, it has been difficult to monitor strain distributions in large or thick composite structures using these point sensors since they can measure only a few or a limited number of points. To overcome this problem, distributed optical-fiber sensors (pulse-pre-pump Brillouin optical-time-domain analysis, PPP-BOTDA) that can measure the strain or temperature distribution along an optical fiber have been developed recently.[12] These are expected to enable strain and temperature distribution monitoring of composite structures.[13,14] The Cure-Hardening Instantaneously Linear Elastic (CHILE) model is the analysis model used to study the residual stresses and curing deformation of composite structures depending on the temperature.[15,16] However, the fundamental validity and applicability of these models have not been proved. Recently, a viscoelastic model has been developed to study the mechanical behavior of polymer composites.[17,18]

This study seeks to clarify the mechanism of strain development in a curing thick composite structure with a temperature distribution in the thickness direction. Strain developed during curing can be separated into two parts according to the cause: chemical-cure shrinkage of the matrix and thermal shrinkage (or expansion) of the cured composite. Therefore, this study consists of a cure-shrinkage part and a thermal-shrinkage part. In both parts, curing is monitored with a distributed optical-fiber sensor (PPP-BOTDA) embedded in a thick laminate and analyzed. In the cure-shrinkage part, two types of analysis (elastic and visco-elastic) were compared to examine the effect of the visco-elastic behavior of a curing composite on strain development.

2. Measurement principles

PPP-BOTDA can measure temperature and strain changes along a measuring optical fiber by observing the frequency shift of Brillouin backscattering light at each point.[19] The measured shift, which is denoted by $\Delta\nu_B$, is a function of the temperature and strain applied at a measuring point and expressed by the following equation:

$$\Delta\nu_B = C_1\Delta\varepsilon + C_2\Delta T \tag{1}$$

where $\Delta\varepsilon$ (ΔT) is the change in applied strain (temperature). C_1 (C_2) is the coefficient of strain (temperature) effect. These two coefficients were determined by preliminary experiments where only a strain or temperature change was applied to an optical fiber. Using this equation, the frequency shift measurement includes both strain and temperature contributions, and hence thermocouples are embedded together for temperature effect compensation. The strains are calculated by the following equation:

$$\Delta\varepsilon = \frac{\Delta\nu_B - C_2\Delta T}{C_1} \tag{2}$$

This study used an NBX-7000 (Neubrex Co., Ltd.) for distributed sensing. The sampling interval (spatial resolution) was 25 mm (20 mm). The measuring precision of the strain was 10 με.

3. Strain distribution in cure-shrinkage process

3.1. Experiment setup

The specimen was made of carbon/epoxy T800S/3900–2B (Toray Industries, Inc.). The stacking configuration was $[90_{80}]$. Figure 1 illustrates the specimen (300 mm long, 100 mm wide and 20 mm thick), indicating the location of an embedded optical fiber for PPP-BOTDA and the thermocouples. The embedded sensors were located between the 8–9, 24–25, 40–41, 56–57, and 72–73 plies (numbered from the bottom) in the thickness direction. The optical-fiber sensor is located at the center of the width direction and perpendicular to the carbon fibers. The thermocouples used for compensation were embedded in the same plies.

The specimen with the embedded sensor was cured in an autoclave. No pressure was applied in order to measure the cure-shrinkage strain accurately. The specimen was heated with only a bottom heating plate to create a temperature distribution in the thickness direction. The temperature history recommended for this material consists of three steps (1, rising by around 2 °C/min from room temperature to 180 °C; 2, holding at 180 °C for 2 h (epoxy curing); and 3, cooling down to room temperature). The main cure shrinkage of the matrix is completed in steps 1 and 2. Therefore, the strain and temperature distribution were measured at intervals of 2 min during these steps.

3.2. Experiment result

Figure 2 presents the temperature histories measured by the embedded thermocouples. The temperature histories in each ply clearly differed. The lower part of the specimen had a higher temperature than the upper part for the overall process. The maximum

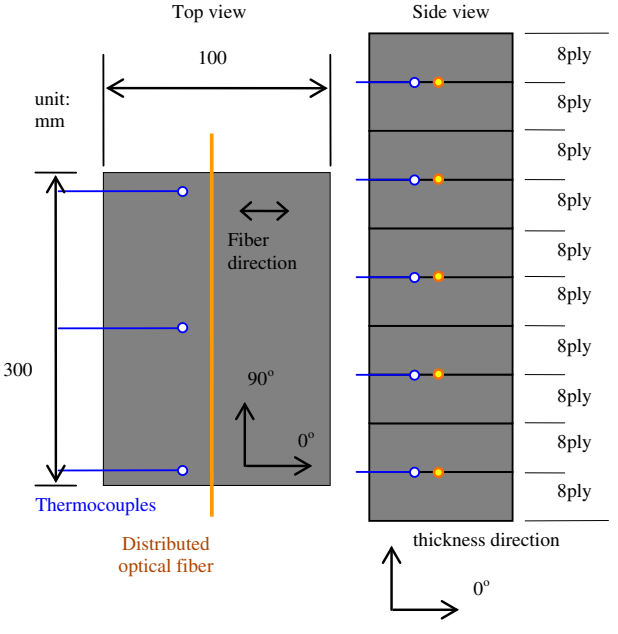

Figure 1. Schematic diagram of specimen with embedded optical-fiber sensors and thermocouples.

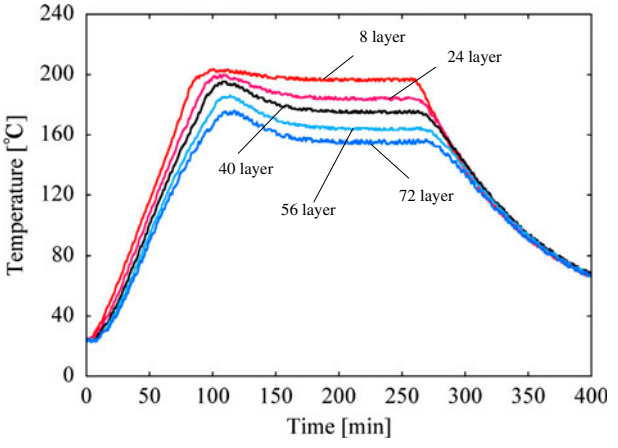

Figure 2. Measured temperature history in thickness direction.

gap between the holding temperature of the 8–9 plies and the 72–73 plies was about 40 °C. Heating with only a bottom plate caused a temperature distribution in the thickness direction. The temperature within a given ply was uniform in this specimen. Such a temperature distribution can occur in thick composite structures regardless of the heating method (hot air and so on).

The strain history in each ply was calculated with Equation (2) using the temperature histories in each ply as temperature compensation for PPP-BOTDA. Each measuring point in the same ply had almost the same strain history, so Figure 3 graphs the calculated strain histories at the center points in each ply. In this graph, each ply had a clearly different strain history. In step 1, the temperature rose and there was less curing. Therefore, the epoxy in the specimen had very low viscosity and the developed stress was relaxed within a fraction of a second. In step 2, the epoxy had visco-elastic or elastic behavior, and the temperature distribution might influence the residual strain and stress distribution. The effect of temperature distribution on the

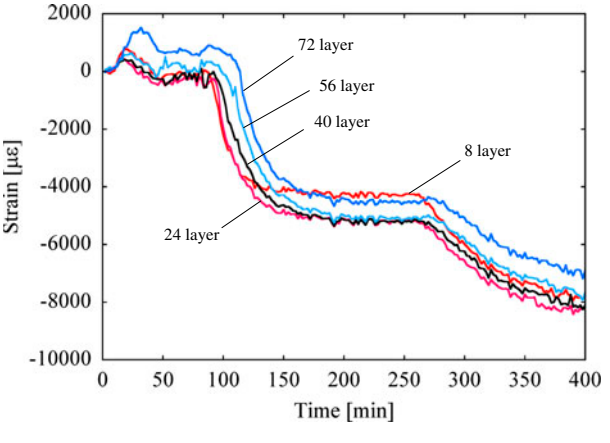

Figure 3. Measured strain history in thickness direction.

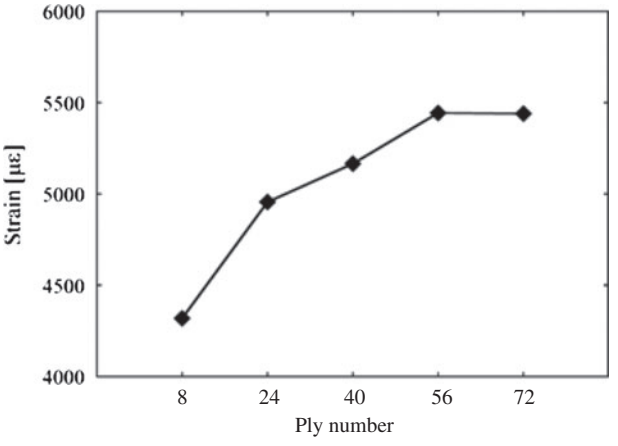

Figure 4. Measured total shrinkage strain in thickness direction.

strain history can be related to two important parameters, the time of cure-shrinkage initiation and the total shrinkage strain during epoxy curing. The cure-shrinkage initiation times differed in each ply. The lower part of the specimen started to shrink sharply before the upper part. When the lower part started to shrink sharply, the upper part was seen to shrink gradually, being affected by the shrinkage of the lower part. The total shrinkage strain in epoxy curing (from 80 to 250 min), which was calculated from Figure 3, is indicated in Figure 4 and ranged from 4200 to 5500 με. The upper part had a greater shrinkage strain than the lower part. The strain of 4200 με in the 8–9 plies was almost the same as that obtained by a preliminary measurement of a thin specimen with a uniform temperature field. When the lower parts started to shrink sharply due to their own cure-shrinkage phenomena, the upper parts had lower viscosity. Accordingly, the shrinkage of the lower parts could affect the total shrinkage of the upper part.

3.3. *Analysis model*

FEM analyses with two different cure models were executed to reveal the cause of the cure-shrinkage strain distribution. One was an 'elastic model' that included a degree-of-curing sub-model, a cure-shrinkage sub-model, and a CHILE model. The other was a 'visco-elastic model' that included a degree-of-curing sub-model (same as the elastic model), a cure-shrinkage sub-model (same as the elastic model), and a visco-elastic cure model established by Kim and White [17,18]. The details of each model are explained later in this section.

Figure 5 indicates the size of the models used for the two analyses. Each model had five parts with different temperature histories corresponding to the temperature histories of the experiment. The lower parts had a higher holding temperature than the upper parts (Figure 5). Figure 6 plots the input temperature histories of each part. The applied temperature histories (as input) were (1) rising in 80 min from room temperature to the holding temperature of each part (160, 170, 180, 190, and 200 °C) and (2) holding for 2 h.

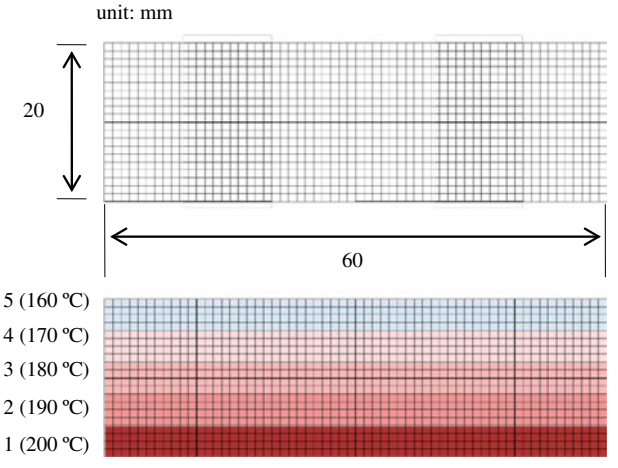

Figure 5. Analytical model and temperature distribution in thickness direction in FEM.

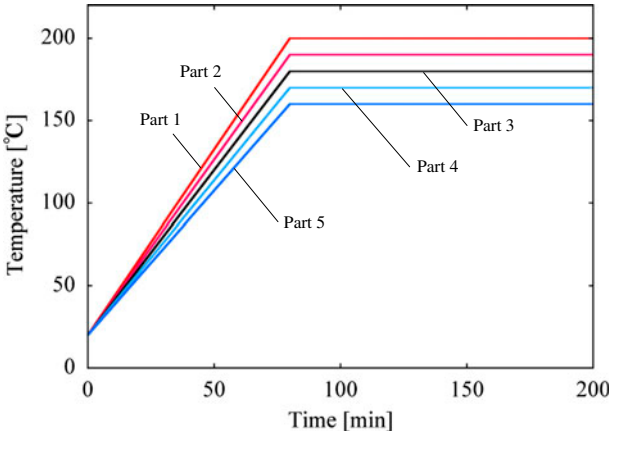

Figure 6. Temperature history at measuring points distributed in thickness direction.

3.3.1. *Model 1 (elastic-curing model)*

The following equations express the degree of cure sub-model.[20]

$$\frac{d\alpha}{dt} = (k_1 + k_2\alpha)\cdot(1-\alpha)\cdot(0.47-\alpha)\ (\alpha \leq 0.3) \tag{3}$$

$$\frac{d\alpha}{dt} = k_3\cdot(1-\alpha)\ (0.3<\alpha) \tag{4}$$

$$k_1 = A_1\cdot\exp\left(-\frac{dE_1}{RT}\right) \tag{5}$$

$$k_2 = A_2 \cdot \exp\left(-\frac{dE_2}{RT}\right) \tag{6}$$

$$k_3 = A_3 \cdot \exp\left(-\frac{dE_3}{RT}\right) \tag{7}$$

In these equations, α and t are the degree of epoxy curing and time. Coefficients k_i, A_i, and E_i ($i = 1$–3) are model parameters determined by experiments with differential scanning calorimetry. R and T are the gas constant and temperature of the material. The following equations express the cure-shrinkage sub-model.

$$\varepsilon_{sh} = 0.0 \ (\alpha < \alpha_{C1}) \tag{8}$$

$$\varepsilon_{sh} = \varepsilon_t \cdot \alpha_S \ (\alpha_{C1} \le \alpha \le \alpha_{C2}) \tag{9}$$

$$\alpha_S = \frac{\alpha - \alpha_{C1}}{\alpha_{C2} - \alpha_{C1}} \tag{10}$$

Here ε_{sh} and ε_t are the cure-shrinkage strain and the total cure-shrinkage strain. α_{c1} and α_{c2} are the degree of curing when resin shrinkage begins and stops. The following equations express the CHILE model.

$$E(\alpha, \xi) = E_0 + (E_c - E_0) \cdot \alpha \tag{11}$$

$$v = 0.3 \tag{12}$$

E, E_0, and E_c are the composite elastic modulus, the composite elastic modulus at very low curing, and the composite elastic modulus at $\alpha = 1.0$. v is the composite Poisson's ratio.

3.3.2. *Model 2 (visco-elastic curing model)*

The following equations express the visco-elastic curing model.[17,18]

$$E(\alpha, \xi) = E_c \cdot \exp\left(-\frac{\xi}{\tau(\alpha)}\right) \tag{13}$$

$$\Delta\xi = \frac{\Delta t}{a_T(\alpha, T)} \tag{14}$$

$$\tau(\alpha) = \tau_0 \cdot 10^{f(\alpha) - (\alpha - 0.98)\cdot(9.9 - \log\tau_0)} \tag{15}$$

$$f(\alpha) = 0.0536 + 0.0615\alpha + 0.9227 \cdot \alpha^2 \tag{16}$$

ξ and t are the reduced time and the stress relaxation time. α_T and τ_0 are the shift factor for time–temperature superposition and the peak relaxation time. In previous modeling, the stress relaxation time was expressed by combining nine different stress relaxation times with nine weight functions. In this study, one representative stress relaxation time was used to simplify the model. All of the values used in these models are summarized in Table 1.

Table 1. Material properties in Section 3.3.

A_1	0.35×10^8/s	ε_t	4.0×10^3 με
A_2	-0.34×10^8/s	α_{c1}	0.6
A_3	0.33×10^5/s	α_{c2}	1.0
dE_1	8.07×10^4 J/mol	E_0	0.08 GPa
dE_2	7.78×10^4 J/mol	E_c	8.0 GPa
dE_3	5.66×10^4 J/mol	ν	0.3
R	8.31 J/mol/K	τ_0	7.94×10^9 min

3.4. *Analysis result*

Figure 7 presents the degree-of-curing histories calculated with the degree-of-curing sub-model (Equations (3) through (7)). The five different temperature histories had different degrees of curing. The degree of curing in the higher-temperature parts increased before that in the lower-temperature parts. Figures 8 and 9 give the calculated strain histories with the elastic cure model and the visco-elastic cure model. Both results exhibited a sudden cure-shrinkage strain drop. With the elastic cure model, the strain was uniform after epoxy curing. In contrast, a strain distribution was obtained after curing with the visco-elastic model. Figure 10 plots the total shrinkage strain values distributed in the thickness direction with the elastic cure model and the visco-elastic cure model. The black line indicates the experiment result. The analytical result with the elastic cure model differed from the experiment result. The one with the visco-elastic cure model had a similar value and trend, with the total shrinkage increasing as a function of the ply number.

To understand these results, we focused on the strain value of the upper part during the 'initiation period'. The initiation period refers to the period when the cure shrinkage of the other part starts (i.e. the degree of curing of the other part exceeded 0.6; see Equation (9) and Table 1) and that of the part in question had not started (i.e. the degree of curing of the part in question was less than 0.6). In the analysis, the time when the degree of curing exceeded 0.6 was 37 min for Part 1 and 47 min for Part 5. Therefore, the strain of Part 5 in this initiation period (10 min) must be generated by shrinkage of the other parts. The shrinkages in the initiation time, calculated by both

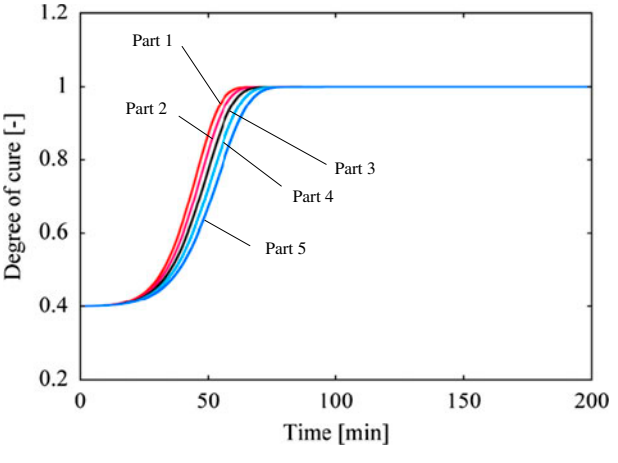

Figure 7. Calculated degree of cure history at measuring points distributed in thickness direction.

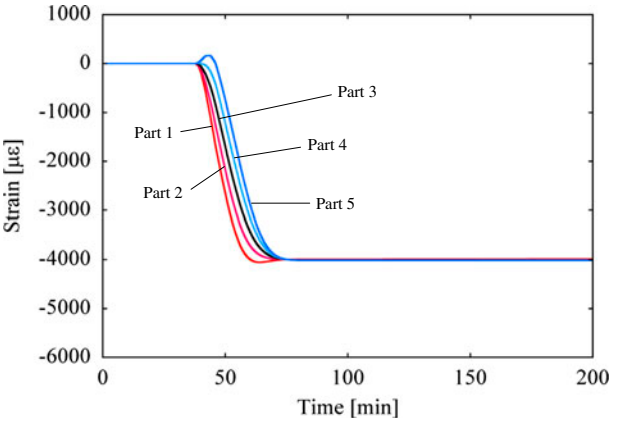

Figure 8. Calculated strain history at measuring points distributed in thickness direction (elastic curing model).

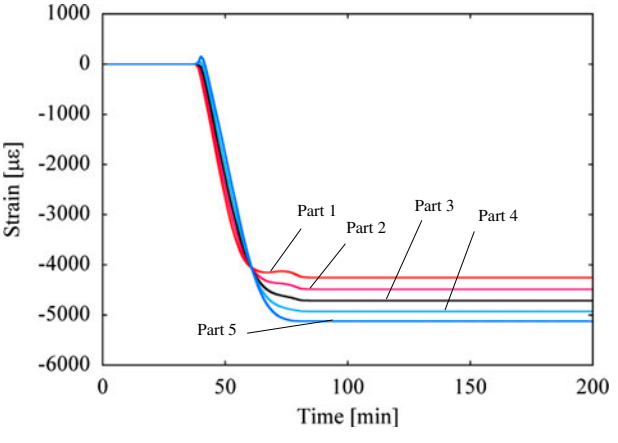

Figure 9. Calculated strain history at measuring points distributed in thickness direction (visco-elastic curing model).

elastic and visco-elastic models, were –116 με (elastic) and –1110 με (visco-elastic). From Figure 3, the experiment value was about –1000 με. In the visco-elastic model, both stress relaxation behavior and a low elastic modulus can make shrinkage in the initiation time higher. These results confirmed that the visco-elastic model can express the material behavior in the 'initiation period' and the total shrinkage strain distribution, and that the elastic cure model cannot.

4. Strain distribution in cooling down process

4.1. Experiment setup

In the previous section, the authors focused on the chemical-cure shrinkage strain, and the strain developed by temperature distribution at steps 1 and 2 was evaluated at atmospheric pressure. This section examines the thermal strain development in step 3, where the material has elasticity.

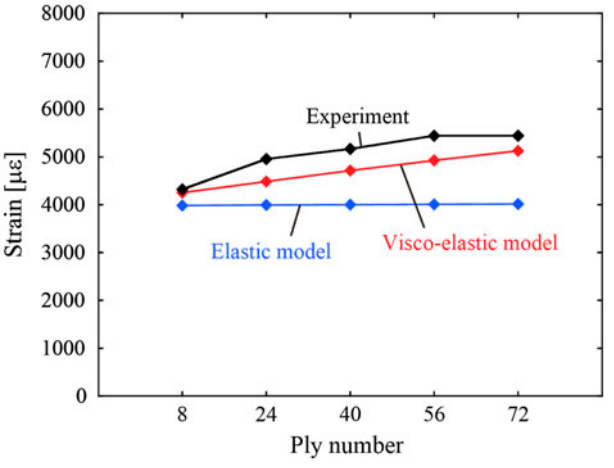

Figure 10. Comparison of total cure-shrinkage strain distributed in thickness direction.

The specimen was made of carbon/epoxy T800S/3900-2B (Toray Industries, Inc.). The stacking configuration was $[90_{80}]$. Figure 11 illustrates the specimen (300 mm long, 100 mm wide and 15 mm thick) and the locations of the embedded optical-fiber sensor and the thermocouples. The embedded sensors were located between the 10–11, 21–22, 50–51, and 70–71 plies in the specimen (numbered from the bottom). The optical fiber is located in the center of the specimen, perpendicular to the carbon fibers. The thermocouples were embedded in the same plies for temperature compensation, and the specimen was cured in an autoclave. The pressure in the autoclave was kept at 0.5 MPa before the cooling step. The specimen was heated with only a bottom heating plate. Before the cooling step, the applied pressure was decreased to atmospheric pressure to relieve the effects of pressure and boundary conditions.

4.2. *Experiment result*

Figure 12 plots the temperature histories measured by the thermocouples embedded in the center of each ply. Plies distributed in the thickness direction had clearly different temperature histories. The lower part of the specimen had a higher temperature than the upper part for the overall curing process. The difference in holding temperatures of the 10–11 plies and the 70–71 plies was 20 °C. The high pressure applied might have produced a smaller difference in holding temperatures compared with the atmospheric pressure result in Section 3.2.

The strain history in each ply was calculated using the measured temperature for compensation. Figure 13 plots the calculated thermal strain histories at the center points distributed in the thickness direction. In this graph, each ply has a clearly different strain history. The total amount of shrinkage strain in the cooling step and the coefficient of temperature expansion (CTE) were calculated from Figure 13. Figure 14 indicates the total strain of each ply. The holding temperature difference resulted in a strain distribution. The amount of the total shrinkage strain decreased as the number of plies increased because a greater temperature change produced higher thermal-shrinkage strain. Figure 15 indicates the apparent CTE values of each ply, calculated directly from

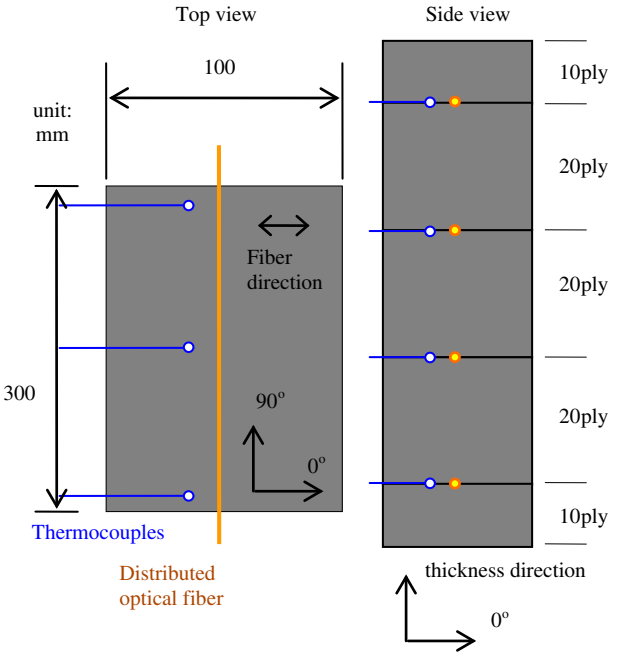

Figure 11. Schematic diagram of specimen with embedded optical-fiber sensors and thermocouples.

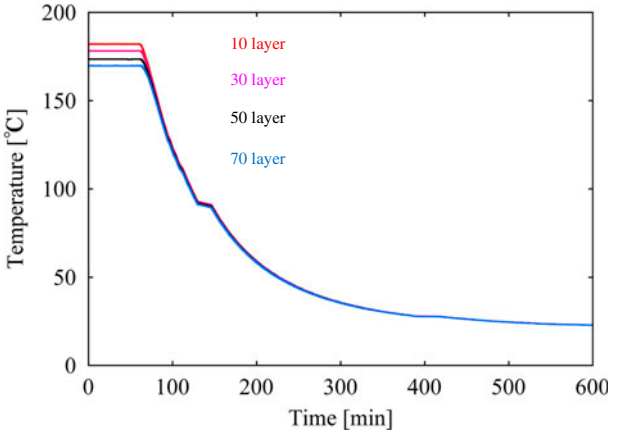

Figure 12. Temperature history at measuring points distributed in thickness direction.

the measured strain and temperature changes. The CTE decreased when the number of plies increased. It is difficult to explain the resulting CTE distribution by temperature change alone. If one part has a smaller temperature change and shrinkage strain (corresponding more plies), that part should have residual compression stress and thus a higher CTE value caused by the other part, which has a greater temperature change and shrinkage strain. To explain the CTE distribution, the fiber volume fraction, V_f, of

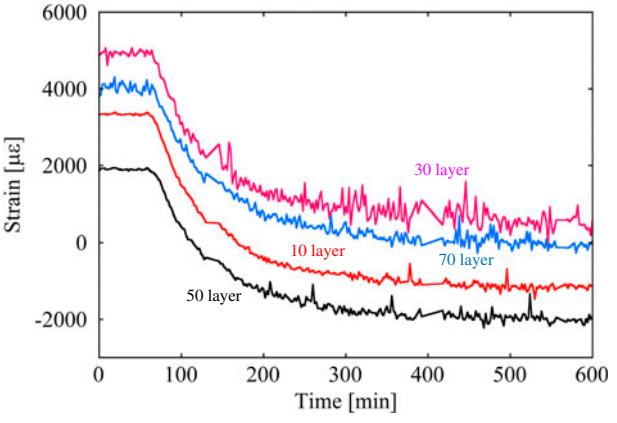

Figure 13. Measured total shrinkage strain in thickness direction.

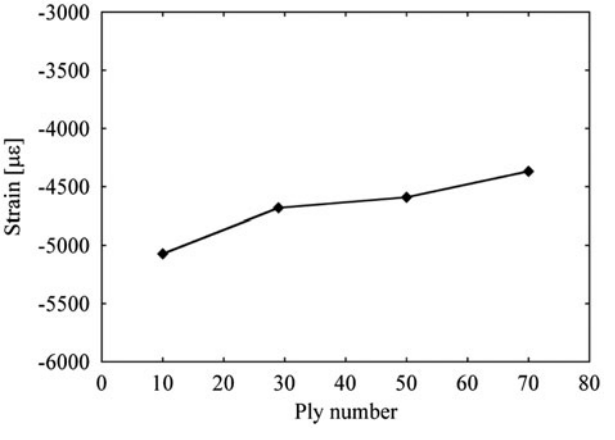

Figure 14. Measured thermal-shrinkage strain distribution in thickness direction.

the cured specimen was measured by microscope observation (VHX-2000, Keyence Corporation). Figure 16 presents one example of a cross-sectional view. The lighter part corresponds to the carbon fibers and the darker part corresponds to the epoxy matrix. In the calculation process of V_f, the fiber part was extracted based on brightness, and the area ratio of the fiber part was defined as V_f. The V_f value of each ply was calculated by averaging date obtained from five different areas ($100 \times 250\ \mu m^2$). Figure 17 plots the calculated V_f distribution. V_f was not uniform in the specimen, and the values increased as a function of the number of plies from the 0th ply to the 60th ply. The V_f values near both the top and bottom surfaces were lower. Air vacuuming both surfaces during curing could have generated resin flows from them.

This result confirmed that the apparent CTE decreased when the number of plies increased. The measured V_f distribution is also considered in the analysis in the next section, together with the temperature distribution. The specimen warped after curing, which was also considered to be caused by the temperature and V_f distribution. Therefore, the warpage is also analyzed in the following section.

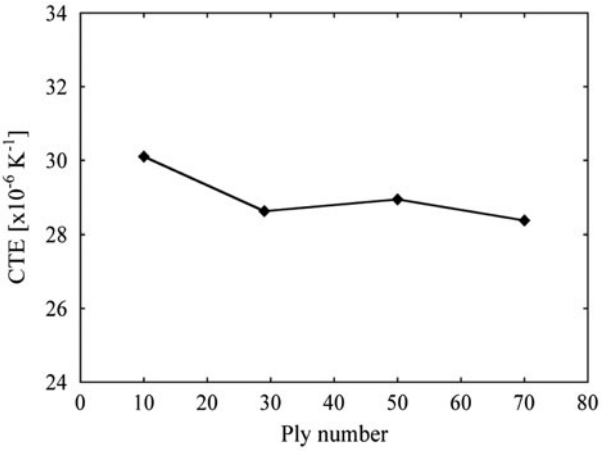

Figure 15. Obtained CTE distribution in thickness direction.

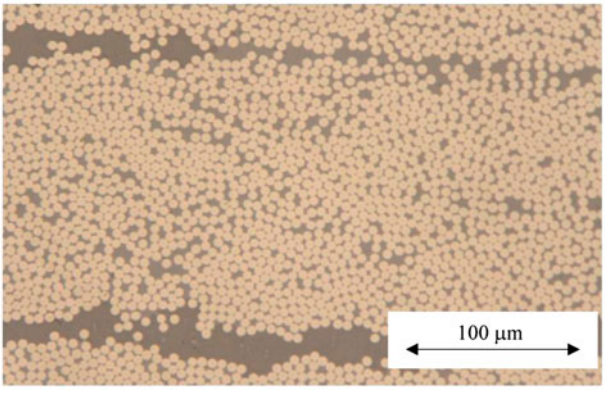

Figure 16. Cross-sectional view of cured specimen.

4.3. *Analysis model*

FEM analyses were conducted with the elastic curing model to determine what caused the thermal-shrinkage strain distribution, CTE, and warping of the cured specimen. Figure 18 indicates the size of the model used for the analysis. The analyses were executed by ABAQUS. Three different analyses were executed to evaluate the effect of the temperature and V_f distribution.

(1) The temperature change was varied in the thickness direction (Figure 12) and V_f was uniform.
(2) The temperature change was uniform and V_f was varied in the thickness direction (Figure 17).
(3) Both the temperature change and V_f were varied in the thickness direction.

The following equations expressed the CTE model including V_f.[21]

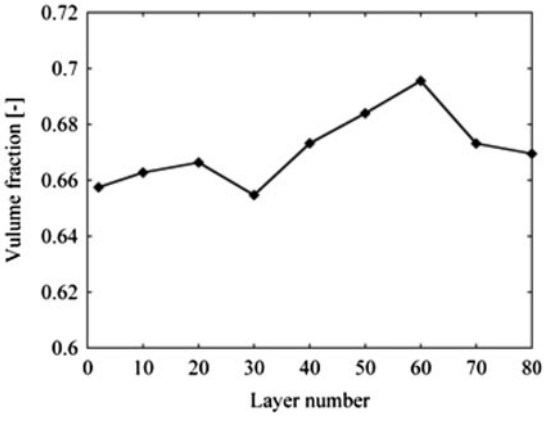

Figure 17. Volume fraction distribution in thickness direction calculated from cross-sectional view.

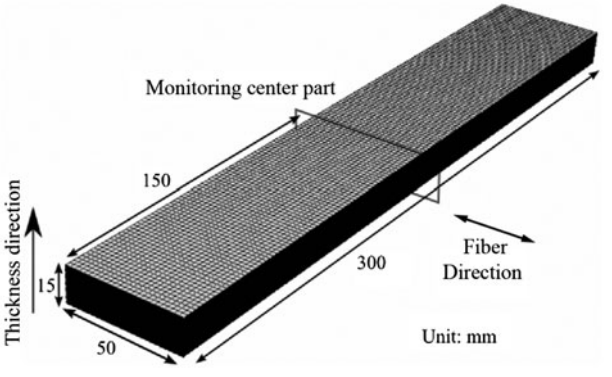

Figure 18. Analysis model for FEM.

$$\alpha_1 = \alpha^m + \frac{V_f}{R}\{E_1^f(\alpha_1^f - \alpha^m)[E^m(1 - {v_{23}}^f - 2v^m{v_{12}}^f)(1 - V_f) + E_2^f(1 + v^m) + E_2^f(1 + v^m)(1 - 2v^m)V_f] + 2E^m E_2^f({\alpha_2}^f - \alpha^m)({v_{12}}^f - v^m)(1 - V_f)\} \tag{17}$$

$$\alpha_2 = \alpha^m + \frac{V_f}{R}\{E_1^f(\alpha_1^f - \alpha^m)(1 - V_f)[E^m(2v_{12}^f + v^m v_{23}^f - v^m) - E_2^f v^m(1 + v^m)] + 2E_2^f(\alpha_2^f - \alpha^m)[E^m(1 - v^m v_{12}^f)(1 - V_f) + E_1^f(1 - v^{m^2})V_f]\} \tag{18}$$

$$R = E^{m^2}(1 - v_{23}^f - 2v_{12}^f v_{12}^f)(1 - V_f)^2 + E^m(1 - V_f)\{E_1^f(1 - v_{23}^f - 4v^m v_{12}^f)V_f + E_2^f[1 + v^m + (1 - v^m)V_f]\} + E_1^f E_2^f(1 + v^m)[1 + (1 - 2v^m)V_f]V_f \tag{19}$$

In these equations, the upper index (f, m) expresses the value for the fiber and matrix. All of the values used in these models are summarized in Table 2.

Table 2. Material properties in Section 4.3.

E_1^f	296.0 GPa	α_1^f	$-3.06 \times 10^{-6}\,K^{-1}$
E_2^f	13.8 GPa	α_2^f	$6.94 \times 10^{-6}\,K^{-1}$
G_{12}^f	9.0 GPa	E^m	3.24 GPa
G_{23}^f	5.8 GPa	G^m	1.19 GPa
v_{12}^f	0.20	v^m	0.36
v_{23}^f	0.25	α^m	$62.0 \times 10^{-6}\,K^{-1}$

4.4. *Analysis result*

Figures 19 and 20 plot the calculated shrinkage strain and the apparent CTE distribution in the thickness direction. The red, blue, and black lines correspond to the results of models (i), (ii), and (iii). The marked points indicate the experiment results. In Figure 19, all three analytical results express the strain increase as a function of ply

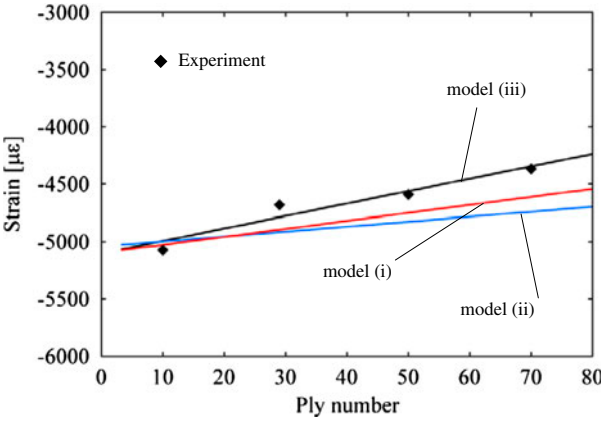

Figure 19. Shrinkage strain distribution in thickness direction.

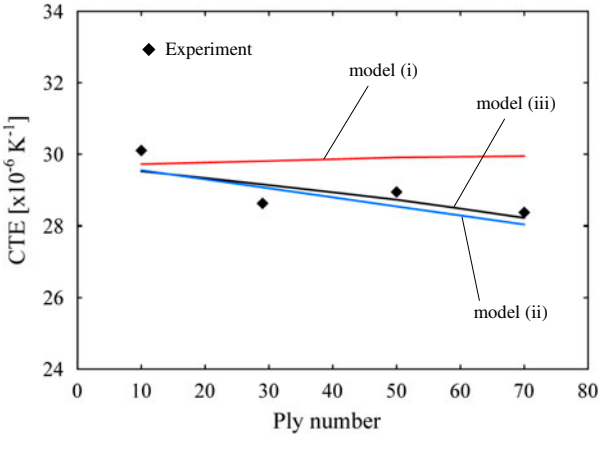

Figure 20. CTE distribution in thickness direction.

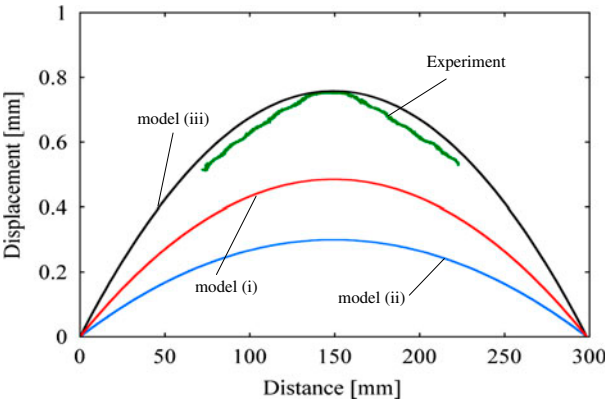

Figure 21. Residual displacement of the bottom surface of specimen.

number. We focused on the maximum strain differences, which are the differences between the shrinkage strain at the 0th ply and that at the 80th ply. The strain difference caused by the temperature distribution (i), V_f distribution (ii), and both the temperature and V_f distribution (iii) were 529, 327, and 827 με. The strain difference caused by the temperature distribution (i) exceeded that caused by the V_f distribution (ii). The result with model (iii) agreed well with the experiment result. Both the temperature and the V_f distribution significantly influenced the shrinkage strain distribution. In Figure 20, the maximum apparent CTE differences caused by the temperature distribution (i), V_f distribution (ii), and both the temperature and V_f distribution (iii) were $0.29 \times 10^{-6}\,\mathrm{K}^{-1}$, $2.02 \times 10^{-6}\,\mathrm{K}^{-1}$, and $1.75 \times 10^{-6}\,\mathrm{K}^{-1}$. The temperature distribution affected the shrinkage strain distribution much less than the V_f distribution. The results with models (ii) and (iii) had similar apparent CTE distributions and agreed well with the experiment result. Based on these results, the apparent CTE value was strongly affected by the V_f distribution. Figure 21 presents the experiment and analytical specimen warpage results obtained at the bottom surface of the cured specimen. The green line represents the experiment result. The result with model (iii) agreed well with the experiment result, confirming that both the temperature and the V_f distribution caused the cured specimen to warp. These results indicate that temperature, strain, and apparent CTE distributions (calculated from temperature and strain) identified by optical-fiber sensors enables predicting the thermal distortion in cured products.

5. Conclusion

This study sought to clarify the mechanism of strain development in curing a thick composite structure with a temperature distribution in the thickness direction. Cure monitoring with an embedded, distributed optical-fiber sensor (PPP-BOTDA) and a cure analysis were performed for both the chemical-cure shrinkage part and the thermal-shrinkage part.

A strain distribution caused by different temperature histories was observed in the chemical-cure shrinkage strain part. The cure-shrinkage initiation times differed in each ply. The higher temperature parts of the specimen started to shrink sharply before the lower temperature parts. The lower temperature parts had more shrinkage strain than

the higher temperature parts. When the higher temperature parts started to shrink sharply due to their own cure-shrinkage phenomena, the lower temperature parts had lower viscosity. Accordingly, the shrinkage of the higher temperature parts could affect the total shrinkage of the lower temperature parts. The visco-elastic model confirmed that the lower viscosity part was influenced by the cure shrinkage of the other part.

The total shrinkage strain, the apparent CTE distribution, and the warpage of the specimen were evaluated in the thermal strain part. FEM analyses with an elastic model were conducted to determine the causes of the thermal-shrinkage strain distribution, the apparent CTE, and the warping of the cured specimen. The model confirmed that both the temperature and the V_f distribution significantly affected the total shrinkage strain and that the temperature distribution had a much smaller effect on the apparent CTE compared with the V_f distribution. Both the temperature and V_f distributions caused the cured specimen to warp. These results indicate that temperature, strain, and apparent CTE distributions (calculated from temperature and strain) identified by optical-fiber sensors can predict thermal distortion in cured products.

Acknowledgments

The authors are grateful for support from the Ministry of Education, Culture, Sports, Science and Technology of Japan under a Grant-in-Aid for Scientific Research (A) (No. 23246146).

References

[1] Bogetti TA, Gillespie JW Jr. Process induced stress and deformation in thick-section thermoset composite laminates. J. Comp. Mater. 1992;26:627–660.
[2] Wisnom MR, Gigliotti M, Ersoy N, Campbell M, Potter KD. Mechanisms generating residual stresses and distortion during manufacture of polymer-matrix composite structures. Composites Part A. 2006;37:522–529.
[3] Zeng X, Raghavan J. Role of tool-part interaction in process-induced warpage of autoclave-manufactured composite structures. Composites Part A. 2010;41:1174–1183.
[4] Lee WI, Loos AC, Springer GS. Heat of reaction, degree of cure, and viscosity of Hercules 3501-6 resin. J. Compos. Mater. 1982;16:510–520.
[5] Bang KG, Kwon JW, Lee DG, Lee JW. Measurement of the degree of cure of glass fiber-epoxy composites using dielectrometry. J. Mater. Process. Technol. 2001;113:209–214.
[6] Doyle C, Martin A, Liu T, Wu M, Hayes S, Crosby PA, Powell GR, Brooks D, Fernando GF. In-situ process and condition monitoring of advanced fibre-reinforced composite materials using optical fibre sensors. Smart Mater. Struct. 1998;7:145–158.
[7] Leng JS, Asundi A. Real-time cure monitoring of smart composite materials using extrinsic Fabry–Perot interferometer and fiber Bragg grating sensors. Smart Mater. Struct. 2002;11:249–255.
[8] Lyon RE, Chike KE, Angel SM. In situ cure monitoring of epoxy resins using fiber-optic Raman spectroscopy. J. Appl. Polym. Sci. 1994;53:1805–1812.
[9] Loleï K, Ruide O, Véronique M, Pascal H. Investigation of process-induced strains development by fibre Bragg grating sensors in resin transfer moulded composites. Composites Part A. 2011;42:274–282.
[10] Mulle M, Collombet F, Olivier P, Zitoune R, Huchette C, Laurin F, Grunevald YH. Assessment of cure-residual strains through the thickness of carbon–epoxy laminates using FBGs Part II: technological specimen. Composites Part A. 2009;40:1534–1544.
[11] Murukeshan VM, Chan PY, Ong LS, Seah LK. Cure monitoring of smart composites using Fiber Bragg Grating based embedded sensors. Sens. Actuators A. 2000;79:153–161.
[12] Kishida K, Li CH. Pulse pre-pump-BOTDA technology for new generation of distributed strain measuring system. In: Ou J, Li H, Daun Z, editors. Structural health monitoring and intelligent infrastructure. London: Taylor & Francis; 2006. p. 471–477.

[13] Minakuchi S, Takeda N, Takeda S, Nagao Y, Franceschetti A, Liu X. Life cycle monitoring of large-scale CFRP VARTM structure by fiber-optic-based distributed sensing. Composites Part A. 2011;42:669–676.
[14] Ito Y, Minakuchi S, Mizutani T, Takeda N. Cure monitoring of carbon–epoxy composites by optical fiber-based distributed strain–temperature sensing system. Adv. Compos. Mater. 2012;21:259–271.
[15] Bogetti TA, Gillespie JW Jr. Process-induced stress and deformation in thick-section thermoset composite laminates. J. Compos. Mater. 1992;26:626–660.
[16] Johnston, AA. An integrated model of the development of process-induced deformation in autoclave processing of composite structures [doctoral thesis]. Vancouver: The University of British Columbia; 1997.
[17] Kim YK, White SR. Stress relaxation behavior of 3501-6 epoxy resin during cure. Polym. Eng. Sci. 1996;36:2852–2862.
[18] Kim YK, White SR. Process-induced residual stress analysis of AS43501-6 composite material. Reinf. Plast. Compos. 1998;16:2–16.
[19] Li C-H, Nishiguchi K, Miyatake M, Makita A, Yokoyama M, Kishita K, Mizutani T, Takeda N. PPP-BOTDA method to achieve 2 cm spatial resolution in Brillouin distributed measuring technique. Tokyo: The Institute of Electronics, Information and Communication Engineers, IEICE Technical report, OFT; 2008.
[20] Lee WI, Loos AC, Springer GS. Heat of reaction, degree of cure, and viscosity of hercules 3501-6 resin. J. Compos. Mater. 1982;16:510–520.
[21] Kyono T, Takahashi K. Theoretical investigation of the thermal expansion coefficients of unidirectional carbon fiber composites. J. Soc. Mater. Sci. 1989;38:307–311.